

José Paulo Marchezi¹, Odim Mendes Jr.¹, Clezio Marcos Denardini¹, Margarete Oliveira Domingues¹ and Nelson Jorge Schuch²

jose.marchezi@inpe.br

¹ National Institute for Space Research - INPE/MCTI, São José dos Campos, SP, Brazil.

² Souther Regional Space Research Center - CRS/INPE - MCTI, Santa Maria, RS, Brazil.

Abstract

In the present study we show the distribution of occurrence of magnetic pulsations PC2, 3, 4 and 5 according to the magnetic latitude and local time over the South American during 2014. The pulsations were obtained from the geomagnetic data collected by the Embrace Magnetometer Network currently installed over Brazil and Argentina covering most of the eastern portion of the South America. Therefore, it covers regions under influence of the Equatorial Electrojet (EE) and the South American Magnetic Anomaly (SAMA). A wavelet based method of analysis was implemented and applied to filter the magnetic data and to provide the dynamic spectra of the magnetic pulsation in order to allow the analysis of non-stationary signals. Considering the results we observed that the PC5 and PC3 have agreed with the current literature with a higher occurrence rates at the higher latitudes and around local noon.

Objectives

Taking into account:

- The Geophysical peculiarities of the South American sector (SAMA, EEJ);
- A network in expansion (Embrace) in the region.

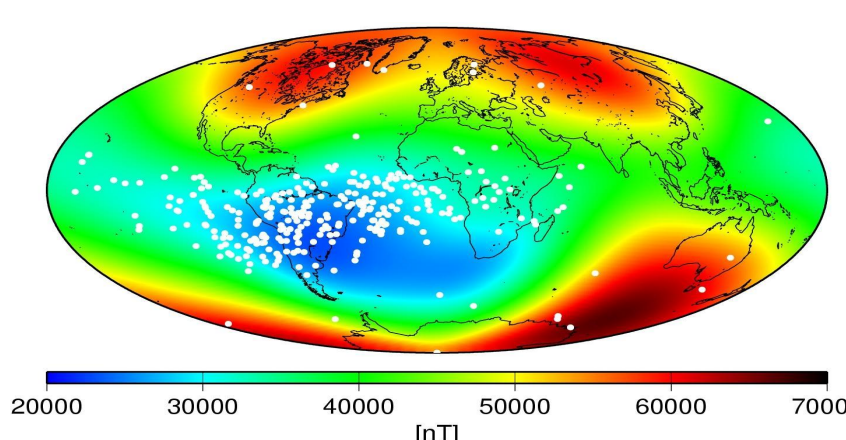


Figure 1: Geomagnetic field intensity, the blue area represents the South American Magnetic Anomaly (SAMA).

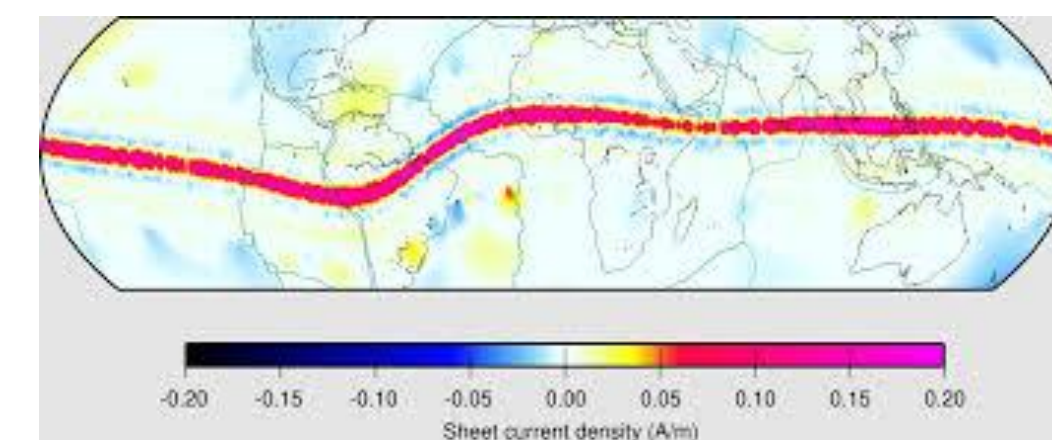


Figure 2: Equatorial Electrojet.

Data and Methodology

At present time, the Embrace magnetometer Network are composed by ten fluxgate sensors. They began to be installed in 2010 at Cachoeira Paulista (CXP) followed by Cuiaba (CBA), Alta Floresta (ALF), Eusébio (EUS), São Luiz (SLZ), Rio Grande (RGA), São José dos Campos (SJC), São Martinho da Serra (SMS), Jataí (JAT) and Vassouras (VSS). Nine are installed over the Brazilian territory and one, RGA, at Argentina. The latitudinal coverage goes from 02° 35'39" S to 53°47'09" S and the longitude, from 38°25'28"W to 67°45'42" W, as shown in the Figure 5.

In this work, 1s-resolution data sets were used, collected from seven stations: CXP, EUS, JAT, RGA, SJC, SLZ, SMS, (identified on the map). Along 2014, the data presented the most continuous extension and better performance (no gaps). The quieter and the more disturbed time intervals were selected according to Kp index, available from WDC, by the Kyoto university. The data were processed and analysed using a wavelet-based method. The wavelet transforms allow a better time-frequency localization concerning to the signal so add a capability of a dynamical data analysis.

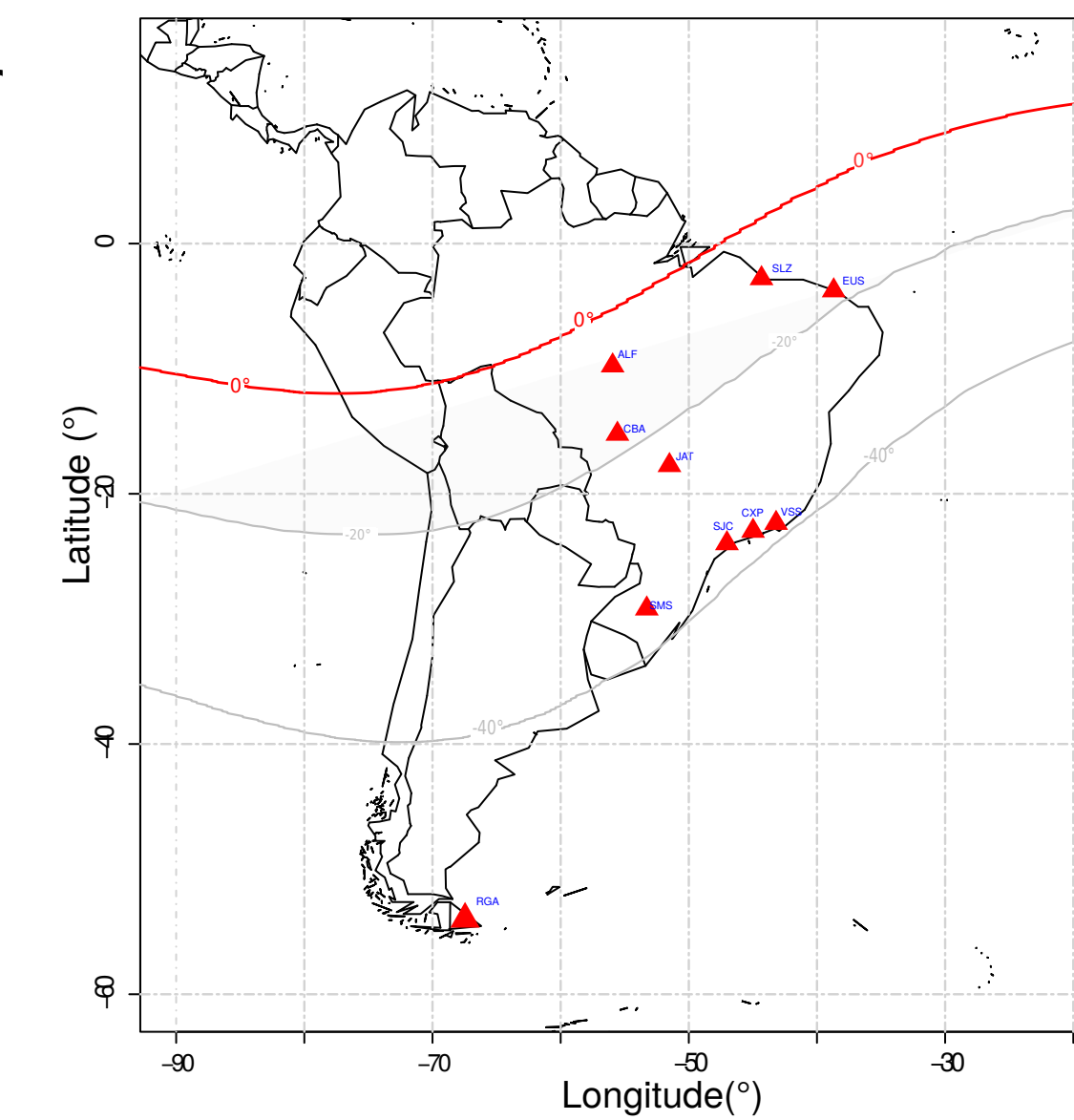


Figure 5: Geographical location of the Embrace magnetometers.

Wavelet analysis

Initially introduced in the early 80s at the last century by the French researcher Jean Morlet for geophysical purposes, this analysis can be applied to non-stationary signals, as the feature of our data.

The wavelet transform can be:

- Continuous (CWT), represented by:

$$W(a, b) = \int_{-\infty}^{\infty} f(t) \bar{\psi}_{a,b}(t) dt \quad a > 0,$$

wavelet function:

$$\psi_{a,b}(t) = \frac{1}{\sqrt{a}} \psi\left(\frac{t-b}{a}\right).$$

or - Discrete (DWT), represented by:

$$d_k^j = 2^j \int_{-\infty}^{\infty} f(t) \psi(2^j t - k) dt.$$

scale function:

$$\phi(x) = 2 \sum_k h(k) \phi(2x - k),$$

wavelet function:

$$\psi(x) = \sum_k g(k) \phi(2x - k),$$

The wavelet functions can be complex or real, symmetric or asymmetric and have compact support or exponential decay and must follow the conditions of admissibility, $\int \psi(t) dt = 0$ and unitary energy, $\int |\psi(t)|^2 dt = 1$.

Figure 6 shows an example of a CWT analysis and the Figure 7 an example of signal decomposition using the DWT.

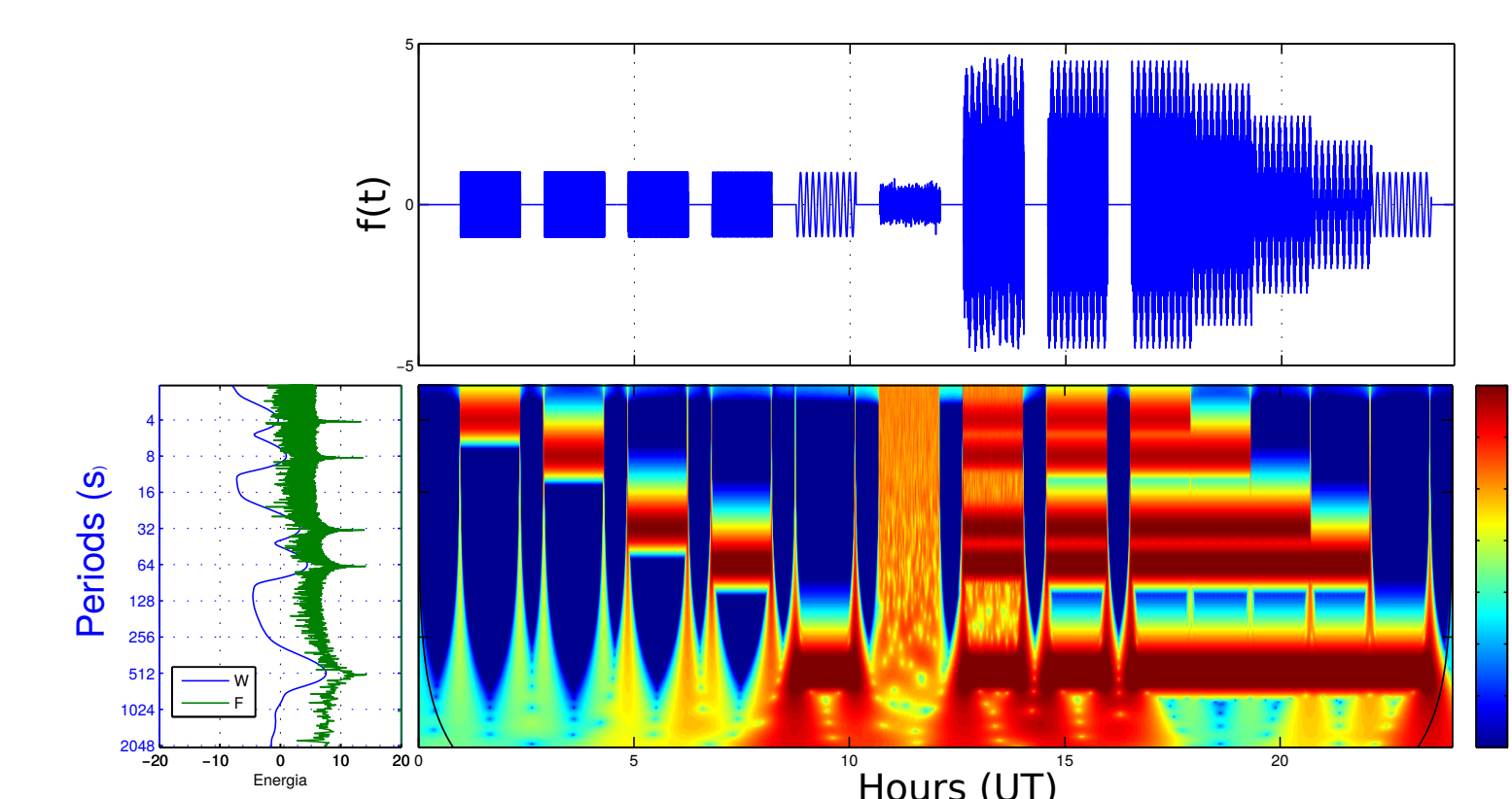


Figure 6: Scalogram of a synthetic signal containing the geomagnetic pulsations band frequencies. The upper panel shows the signal, in the middle is the scalogram and the left panel is the global wavelet spectrum superimposed by the Fourier spectrum (based on the original Odim Mendes's plot).

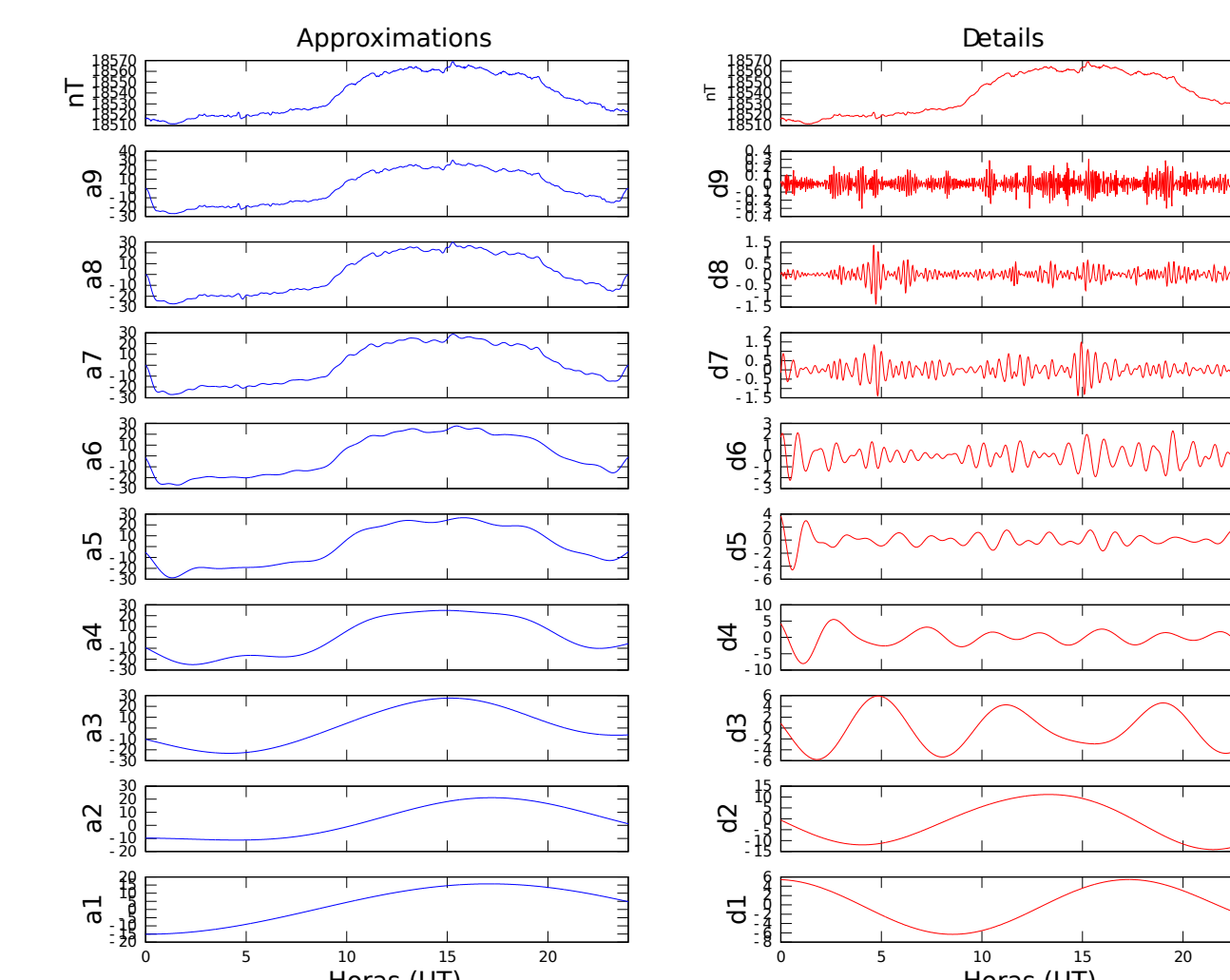


Figure 7: H component of a magnetometer decomposed into approximation levels and their respective details using the Meyer discrete orthogonal wavelet transform.

Results and Discussions

In order to identify the frequencies in the signals, the CWT with Morlet analysing function was applied to the H component for all stations. As examples, scalograms are shown in Figures 8 and 9. The black lines identify the pulsation frequency ranges.

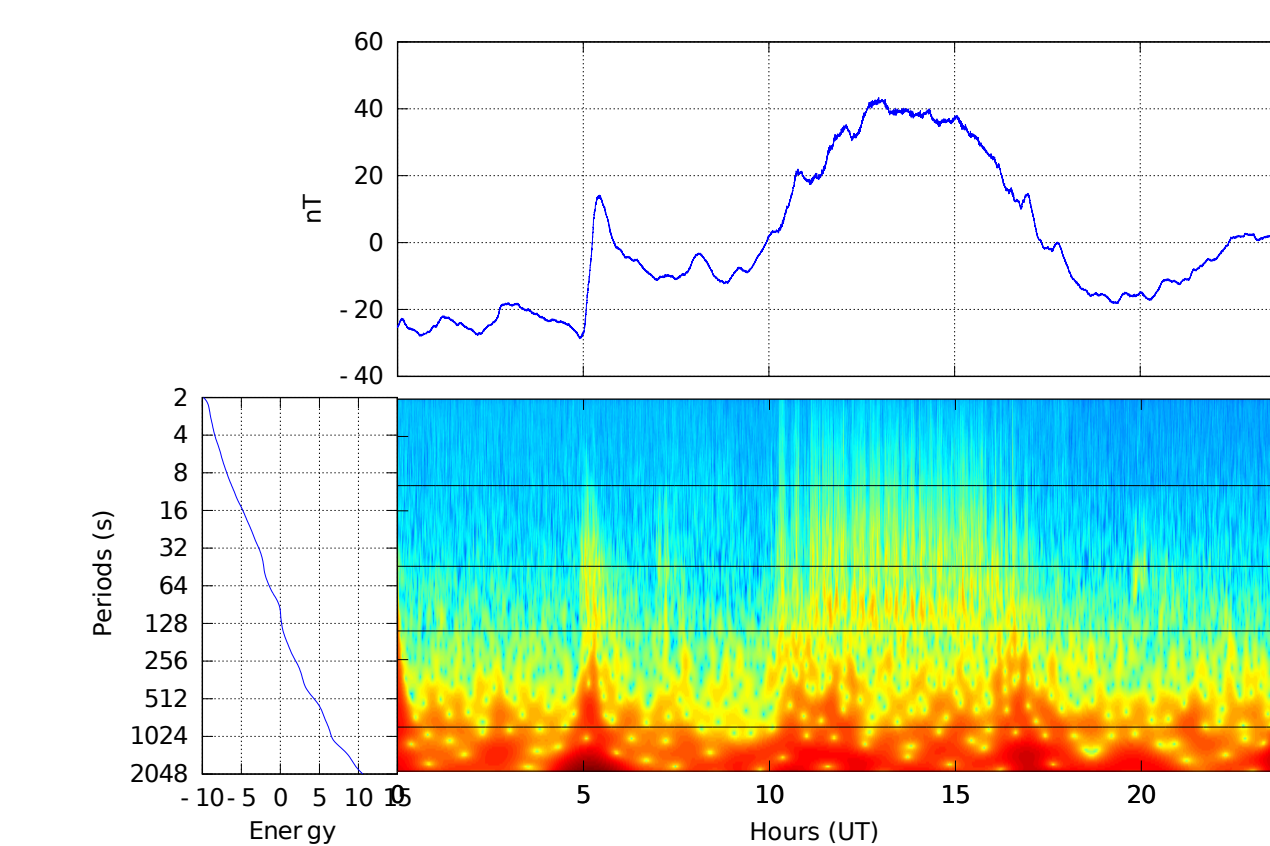


Figure 8: Scalogram of H Component for the Eusébio station at 2014, August 28.

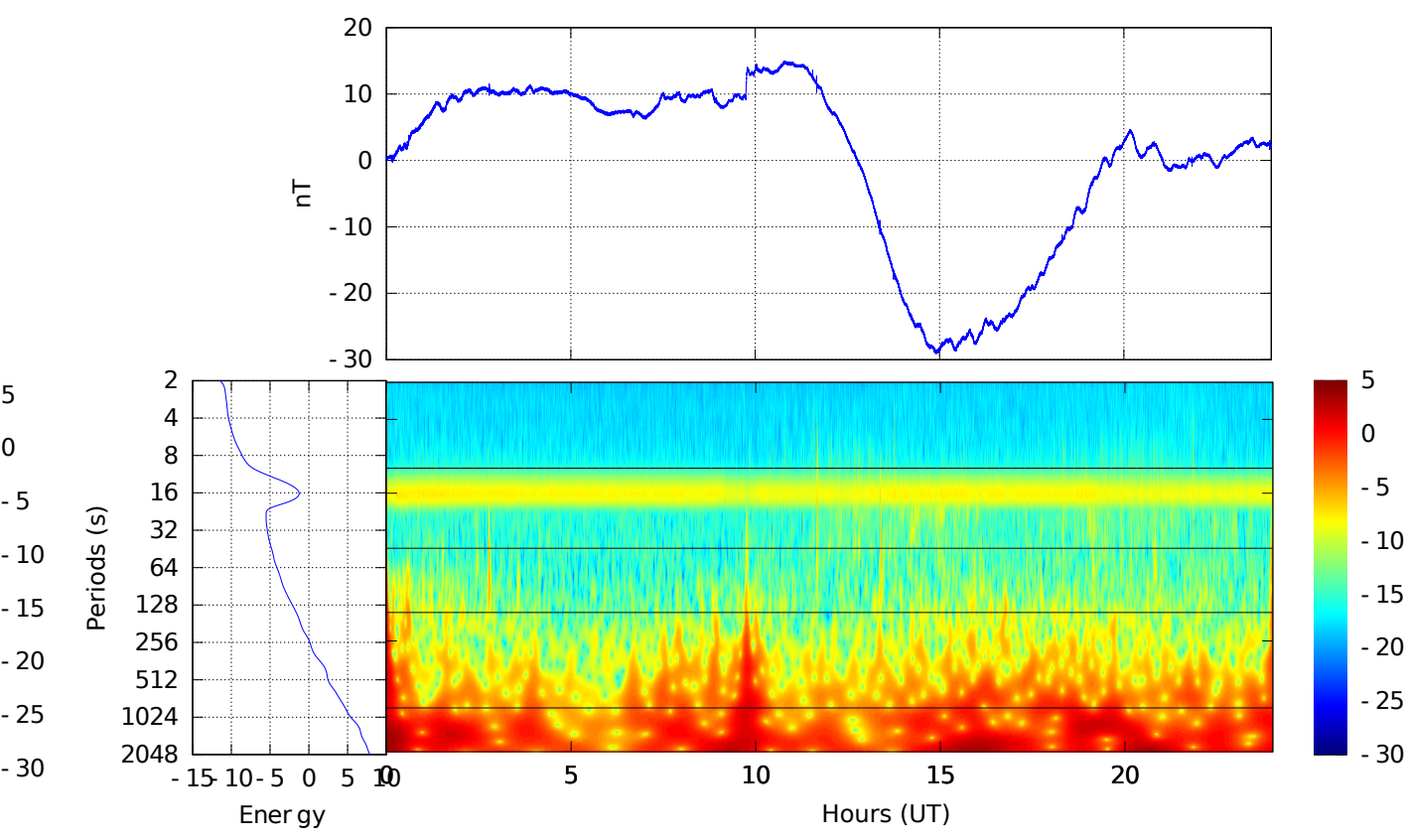


Figure 9: Scalogram of H Component for the Eusébio station at 2014, February 13.

We can see in Figure 8 many structures, from the lower frequencies to the higher ones around local mid-day. Different from figure 9, the latter does not show those structures, but a continuous frequency band during all day. It represents the capability of the wavelet to see different frequency bands, that allows the perception of an possible external noise in the signal in Figure 9. The total variation was filtered using the DWT with Meyer orthogonal wavelet and a dynamic map was created showing the amplitude of the pulsations according to the local time and the latitude. Figure 10 is for quiet days and Figure 11 disturbed days.

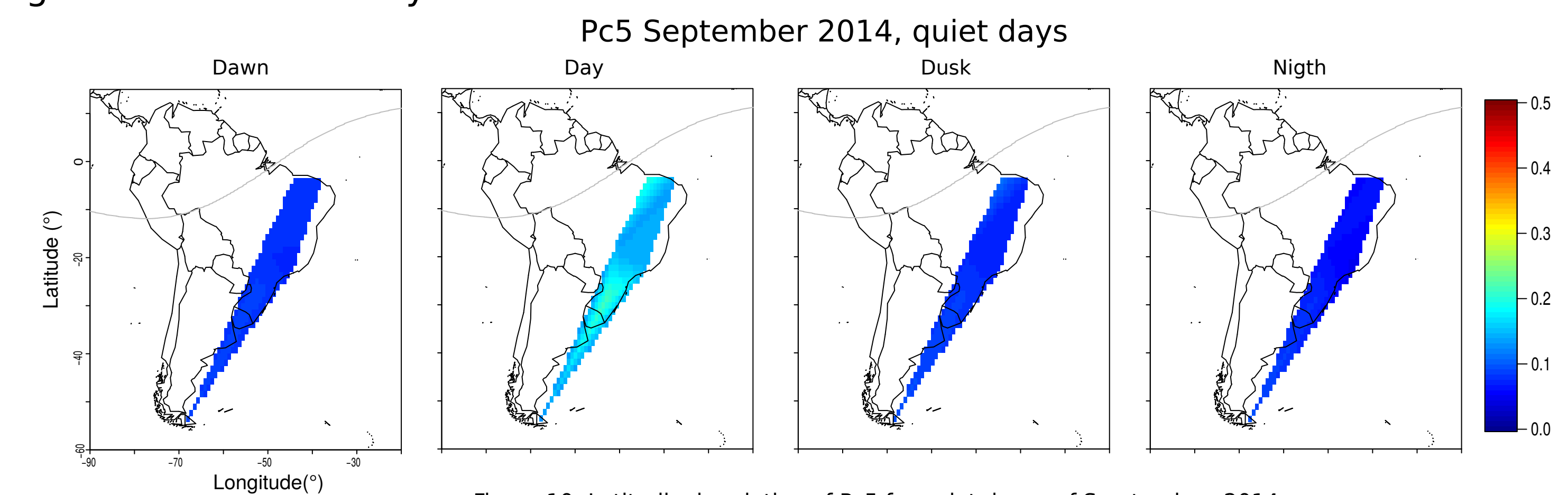


Figure 10: Latitudinal variation of Pc5 for quiet days of September, 2014.

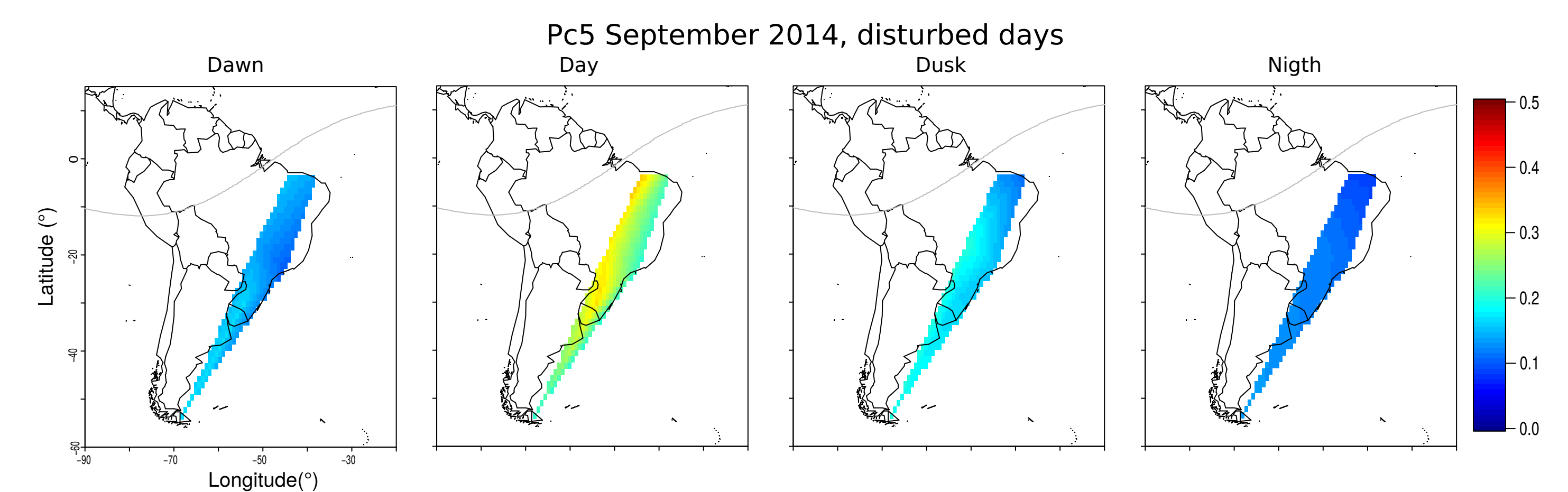


Figure 11: Latitudinal variation of Pc5 for disturbed days of September, 2014.

Those figures are examples of the visual representation of the amplitudes of pulsations. In them, it is shown the mean amplitude for the signal in September 2014. We can see that the amplitude of the Pc5 signal is bigger for disturbed days than for the calm days, and an increase in the amplitude is seen about the local mid-day in both cases.

Aknowledgements

Marchezi J. P. thanks Capes and CNPq/MCTI (134331/2014 - 1), O.M. and M.O.D. also thank the Brazilian CNPq agency (CNPq 312246/2013-7, 306038/2015-3) for the grants. The authors thank the Brazilian Space Weather Program (Embrace - INPE/MCTI) for the data used.

Introduction

Geomagnetic pulsations, as current term, designate the short period variations observed in magnetograms during geomagnetic storms, according to the initial idea of Stewart (1861). These oscillations are primarily manifestations of hydromagnetic waves of very low frequency (ULF), generated by a variety of processes and plasma instabilities related to the dynamical interaction between the solar wind and the magnetosphere-ionosphere system. The pulsations are classified into two main types according to its waveform and period. Oscillations with nearly sinusoidal waveform were called continuous pulsations (Pc), and fluctuations with more irregular shape were called irregular pulsations (Pi). Nowadays, they were also divided into seven subgroups according to the band period of the oscillations.

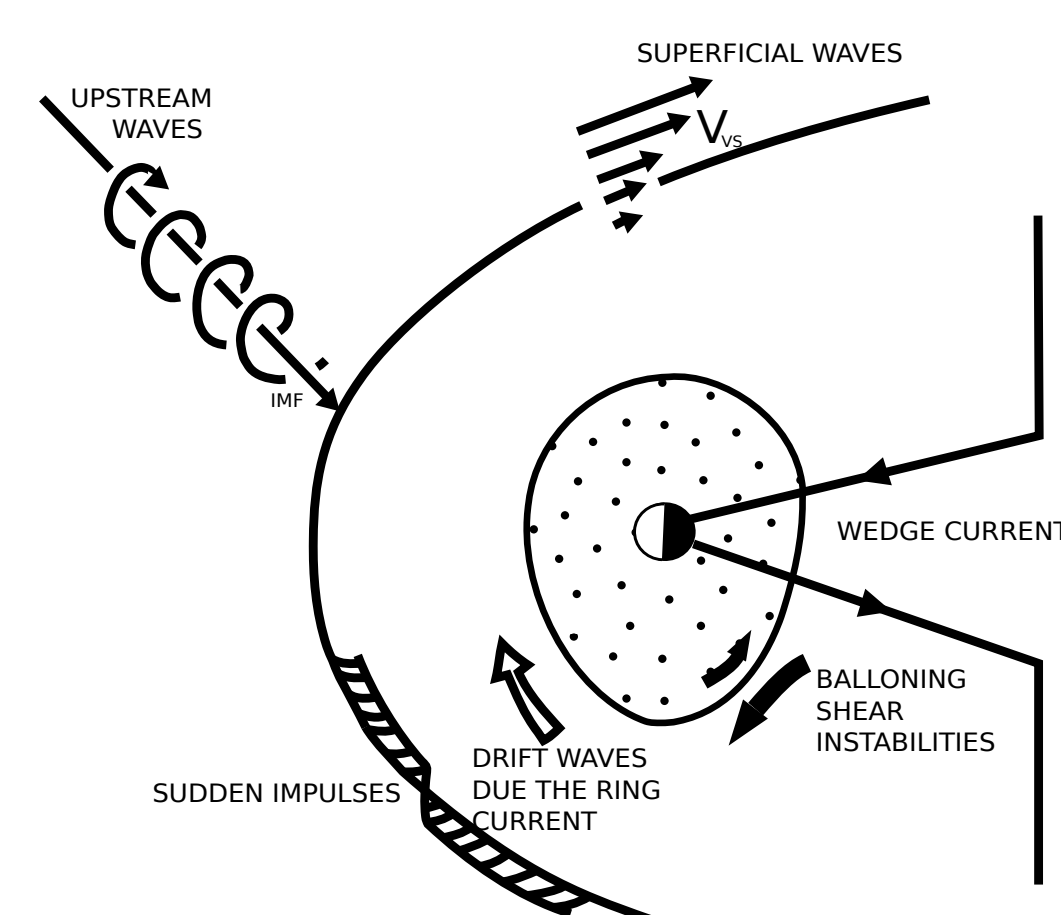


Figure 3: Main sources of excitation of internal and external MHD waves. Source: Yumoto, 1988.

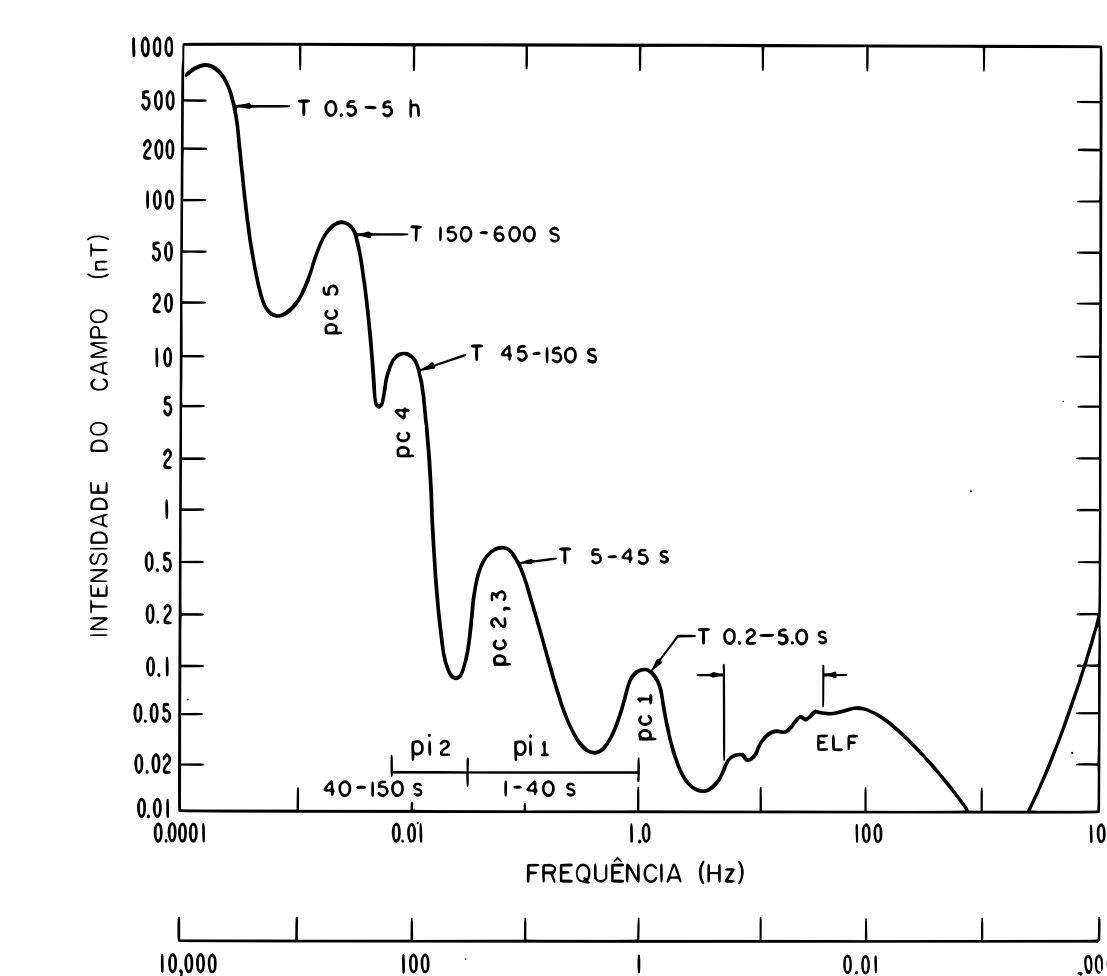


Figure 4: Amplitude spectrum of geomagnetic pulsations as a function of frequency. Source: Campbell, 2003.